Coherent control of macroscopic quantum states in a single-Cooper-pair box

Y. Nakamura*, Yu. A. Pashkin† & J. S. Tsai*

* *NEC Fundamental Research Laboratories, Tsukuba, Ibaraki 305-8051, Japan*
† *CREST, Japan Science and Technology Corporation (JST), Kawaguchi, Saitama 332-0012, Japan*

....

A nanometre-scale superconducting electrode connected to a reservoir via a Josephson junction constitutes an artificial two-level electronic system: a single-Cooper-pair box. The two levels consist of charge states (differing by 2*e*, where *e* is the electronic charge) that are coupled by tunnelling of Cooper pairs through the junction. Although the two-level system is macroscopic, containing a large number of electrons, the two charge states can be coherently superposed[1–4]. The Cooper-pair box has therefore been suggested[5–7] as a candidate for a quantum bit or 'qubit'—the basic component of a quantum computer. Here we report the observation of quantum oscillations in a single-Cooper-pair box. By applying a short voltage pulse via a gate electrode, we can control the coherent quantum state evolution: the pulse modifies the energies of the two charge states non-adiabatically, bringing them into resonance. The resulting state— a superposition of the two charge states—is detected by a tunnelling current through a probe junction. Our results demonstrate electrical coherent control of a qubit in a solid-state electronic device.

Rapidly improving nanofabrication technologies have made quantum two-level systems in solid-state devices promising for functional quantum circuit integration. To coherently control an individual two-level system as a unit of such circuits, several systems have been examined, such as electronic[8–10] and spin[11] states in quantum dots, nuclear spins of impurity atoms embedded in a substrate[12], and magnetic-flux states in a superconducting ring[13,14]. However, only optical coherent control has been realized experimentally[10].

A single-Cooper-pair box[1] (Fig. 1) is a unique artificial solid-state system in the sense that: (1) although there are a large number of electrons in the metal 'box' electrode, under superconductivity they all form Cooper pairs and condense into a single macroscopic ground state, $|n\rangle$, separated by a superconductivity gap Δ from the excited states with quasiparticles. (Here $|n\rangle$ denotes the charge-number state with the excess number of electrons n the box, *n*.) (2) The only low-energy excitations are the transitions between different $|n\rangle$ states due to Cooper-pair tunnelling through the Josephson junction, if Δ is larger than the single-electron charging energy of the box E_C. (3) E_C, if larger than the Josephson energy E_J and the thermal energy k_BT, suppresses a large fluctuation of *n*. Hence, we can consider the system an effective two-level system by taking into account the two lowest-energy states which differ by one Cooper pair. (4) In addition, the relative energy of the two levels can be controlled through the gate voltage. For example, as shown in Fig. 2a, the electrostatic energies, $E_C(n - Q_t/e)^2$, of two such charge states $|0\rangle$ and $|2\rangle$ change as a function of the total gate-induced charge Q_t and cross each other at $Q_t/e = 1$. (The parabolic background energy is subtracted.) In the presence of Josephson coupling, and with weak enough dissipation[15], these charge states would be coherently superposed and form two anticrossing eigen-energy bands (dashed curves in Fig. 2a). The existence of the coherence has been inferred in energy-domain experiments by measuring ground-state properties[1,2] and by spectroscopy[3,4]. However, coherent control and observation of quantum-state evolution

in the time domain has not been achieved. Such time-domain techniques are necessary to enable applications based on quantum coherent evolution[5–7].

To investigate the coherent evolution, we applied a sharp voltage pulse to the pulse gate to control energy levels of the charge states and to manipulate the quantum state as shown in Fig. 2a and b. If we select an initial condition $Q_t = Q_0$ far to the left from the resonance point (where Q_0 is the d.c.-gate induced charge), the initial state would, with a large probability ($\sim$1), be the ground state which is almost the pure $|0\rangle$ state. The pulse brings the two charge states into resonance and lets the wavefunction coherently evolve between $|0\rangle$ and $|2\rangle$ during the pulse length Δt. The quantum state at the end of the pulse would be a superposition of the two charge states which depends on Δt. Here, the rise and fall times of the pulse must be short compared to the coherent oscillation time h/E_J, otherwise the state just follows the ground-state energy band adiabatically.

The probe junction was voltage-biased with an appropriate voltage V_b so that $|2\rangle$ decays to $|0\rangle$ with two sequential quasiparticle tunnelling events through the probe junction with predictable rates Γ_{qp1} and Γ_{qp2} (about $(6\,\text{ns})^{-1}$ and $(8\,\text{ns})^{-1}$ in the present experiment); $|0\rangle$ is stable against the quasiparticle tunnelling[4]. The role of the quasiparticle tunnelling is twofold. One is the detection of $|2\rangle$ as two tunnelling electrons. As this 'detector' is always connected to the two-level system even during the pulse, a large probe junction resistance R_b is necessary for small Γ_{qp1} ($\propto R_b^{-1}$) to avoid excessively disturbing the coherence. The other role is the preparation of the initial state for the next pulse operation by relaxation to the ground state. With an array of pulses with a repetition time T_r longer than the relaxation time, we can repeat the pulse operation many times and measure the direct current through the probe junction which would reflect the population in $|2\rangle$ after each pulse operation.

In the experiment, the actual pulse height at the pulse gate was not measurable, so we swept the range of d.c.-induced charge Q_0, with a fixed pulse height and the repetition time T_r. Figure 2c shows the current through the probe junction versus Q_0. Without a pulse array (dashed line), a broad current peak appeared at $Q_0/e = 1$ where charge states $|0\rangle$ and $|2\rangle$ are degenerate. This current is the
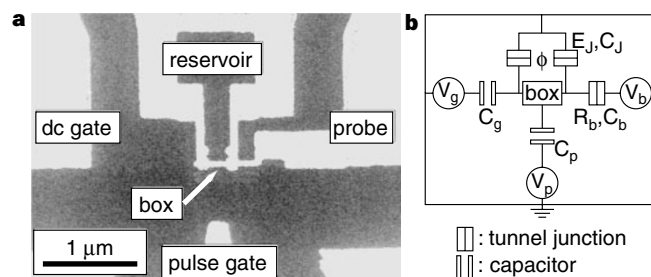

Figure 1 Single-Cooper-pair box with a probe junction. **a**, Micrograph of the sample. The electrodes were fabricated by electron-beam lithography and shadow evaporation of Al on a SiN_x insulating layer (400-nm thick) above a gold ground plane (100-nm thick) on the oxidized Si substrate. The 'box' electrode is a $700 \times 50 \times 15$ nm Al strip containing $\sim 10^8$ conduction electrons. The reservoir electrode was evaporated after a slight oxidation of the surface of the box so that the overlapping area becomes two parallel low-resistive tunnel junctions ($\sim$10 kΩ in total) with Josephson energy E_J which can be tuned through magnetic flux ϕ penetrating through the loop. Before the evaporation of the probe electrode we further oxidized the box to create a highly resistive probe junction ($R_b \approx 30$ MΩ). Two gate electrodes (d.c. and pulse) are capacitively coupled to the box electrode. The sample was placed in a shielded copper case at the base temperature ($T \approx 30$ mK; $k_BT \approx 3\,\mu$eV) of a dilution refrigerator. The single-electron charging energy of the box electrode $E_C \equiv e^2/2C_\Sigma$ was $117 \pm 3\,\mu$eV, where C_Σ is the total capacitance of the box electrode. The superconducting gap energy Δ was $230 \pm 10\,\mu$eV. **b**, Circuit diagram of the device. The *C*s represent the capacitance of each element and the *V*s are the voltage applied to each electrode.

Josephson-quasiparticle (JQP) current[16,17] and is carried by a cyclic process consisting of one Cooper-pair tunnelling between the two charge states and two sequential quasiparticle tunnelling events at the probe junction. When applying a pulse array (solid line), on the left side of the JQP peak we observed a pulse-induced current with several peaks whose positions did not depend on T_r but on Δt. In Fig. 3a we extract the pulse-induced part of the current, ΔI, for the pulse length $80 \leqslant \Delta t \leqslant 450$ ps. With increasing Δt, all the peaks moved towards smaller Q_0 and disappeared at $Q_0/e \approx 0.5$. The region where the peaks existed extended to smaller Q_0 linearly with increasing pulse height (data not shown).

We simulated the pulse operation of the quantum state by numerically solving a time-dependent Schrödinger equation. We calculated the average increase in the probability density at $|2\rangle$ after a single-pulse operation, $\langle \Delta P(2) \rangle$, which should approximately be proportional to ΔI. To adjust the maximum oscillation period in the time domain, T_{coh}, we used a Josephson energy $E_J = 51.8$ μeV, and to adjust $Q_0(= 0.51e)$ where T_{coh} was observed we used an effective pulse height $\Delta Q_p/e$ of 0.49. The overall features of the pulse-induced current were reproduced (Fig. 3b). The value of Q_0 where T_{coh} was observed corresponded to the point where the applied pulse brought the two levels into resonance and T_{coh} equalled h/E_J. The oscillation period in the time domain changed according to $h/\sqrt{E_J^2 + \delta E^2}$, where $\delta E \equiv 4E_C[(Q_0 + \Delta Q_p)/e - 1]$ is the electrostatic energy difference between the two charge states during the pulse.
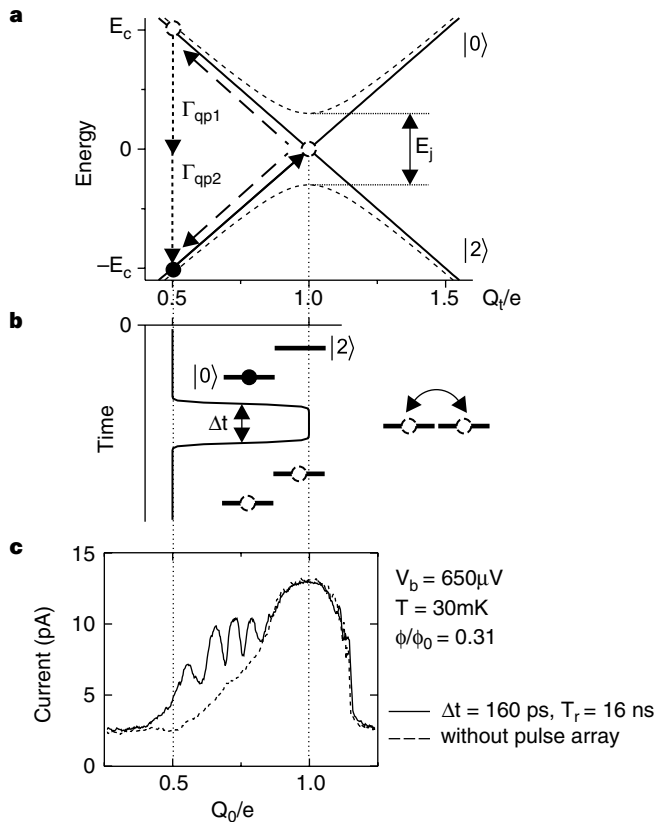
Figure 2 Pulse modulation of quantum states. **a**, Energy diagram illustrating electrostatic energies (solid lines) of two charge states $|0\rangle$ and $|2\rangle$ (with the number of excess charges in the box $n = 0$ and 2) as a function of the total gate-induced charge $Q_t \equiv Q_0 + C_p V_p(t)$, where $Q_0 = C_g V_g + C_b V_b$ is the d.c.-gate induced charge. The dashed curves show eigenenergies (in the absence of the quasiparticle tunnelling at the probe junction) as a function of Q_t. Suppose that before a pulse occurs, Q_t equals Q_0, which is far from the resonance point, and the system is approximately in the pure charge state $|0\rangle$ (filled circle at lower left). Then, a voltage pulse of an appropriate height abruptly brings the system into resonance $Q_t/e = 1$ (solid arrow), and the state starts to oscillate between the two charge states. At the end of the pulse, the system returns to $Q_t = Q_0$ (dashed arrow) with a final state corresponding to the result of the time evolution. Finally, the $|2\rangle$ state decays to $|0\rangle$ with two quasiparticle tunnelling events through the probe junction with rates of Γ_{qp1} and Γ_{qp2} (dotted arrows). **b**, Schematic pulse shape with a nominal pulse length Δt (solid line). The rise/fall times of the actual voltage pulse was about 30–40 ps at the top of the cryostat. The voltage pulse was transmitted through a silver-plated Be-Cu coaxial cable (above 4.2 K), a Nb coaxial cable (below 4.2 K) and an on-chip coplanar line to the open-ended pulse gate shown in Fig. 1a. The insets illustrate situations of the energy levels before/during/after the pulse. **c**, Current through the probe junction versus Q_0 with (solid line) and without (dashed line) the pulse array. The pulse length was $\Delta t = 160$ ps and the repetition time was $T_r = 16$ ns. The data were taken at $V_b = 650$ μV and $\phi/\phi_0 = 0.31$, where $\phi_0 \equiv h/2e$ is a flux quantum.
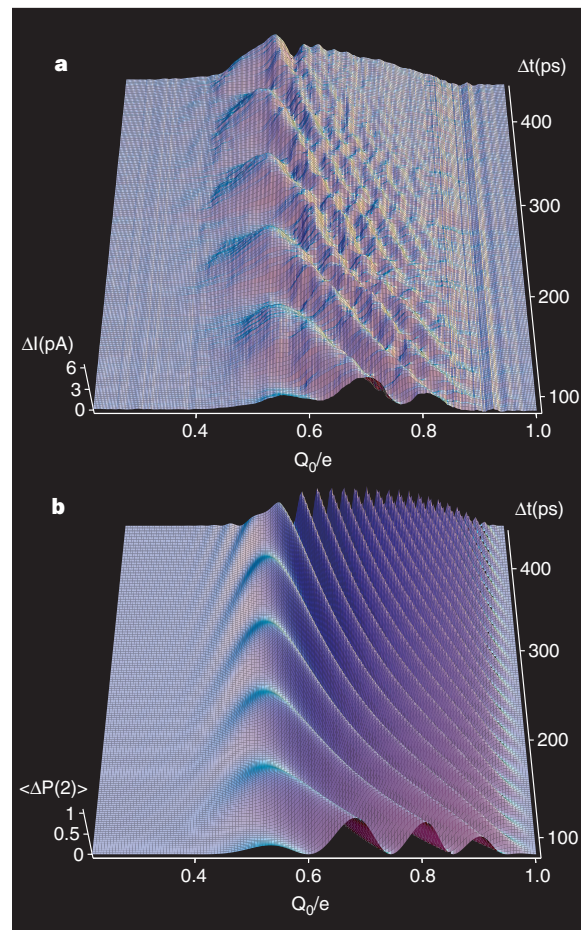
Figure 3 Effect of applying pulses as a function of d.c.-induced charge Q_0 and pulse length Δt. **a**, Three-dimensional plot of pulse-induced current ΔI which is the difference between currents measured with and without a pulse array. $\Delta t = 80$ ps was the shortest pulse length available with our pulse-pattern generator (Anritsu MP1758A). **b**, Calculated average increase in probability density at $|2\rangle$ after a single-pulse operation, $\langle \Delta P(2) \rangle$. The averaged probability density after the pulse was calculated by numerically solving a time-dependent Schrödinger equation and by averaging out small residual oscillations in the time domain. The effect of decoherence was not included. As the initial condition of the Schrödinger equation, we used a mixture of two eigenstates at $Q_t = Q_0$ with weights obtained from a steady-state solution of density-matrix equations that describe charge transport through the device in the absence of a pulse array. The initial probability density was also calculated from the steady-state solution. In the calculations, Josephson energy $E_J = 51.8$ μeV and an effective pulse height $\Delta Q_p/e = 0.49$ were used. The solid line in Fig. 2b shows an example (at $\Delta t = 300$ ps) of the pulse shape used in this calculation.
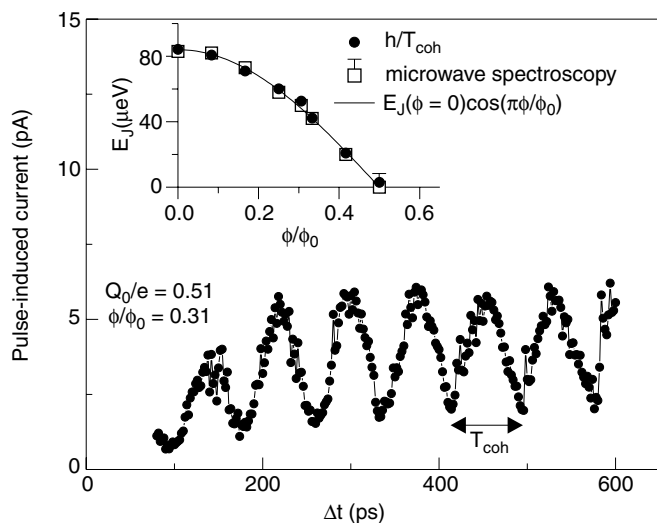
Figure 4 Pulse-induced current as a function of the pulse length Δt. The data correspond to the cross-section of Fig. 3a at $Q_0/e = 0.51$. Inset, Josephson energy E_J versus the magnetic flux ϕ penetrating through the loop. E_J was estimated by two independent methods. One was from the period of the coherent oscillation T_{coh} as h/T_{coh}. The other was from the gap energy observed in microwave spectroscopy[4]. The solid line shows a fitting curve with $E_J(\phi = 0) = 84$ μeV assuming cosine ϕ-dependence of E_J.

Figure 4 shows the pulse-induced current at $Q_0/e = 0.51$ as a function of Δt, showing that the coherent oscillation can be observed in the time domain and that we can control the quantum state through an arbitrary pulse length Δt. The oscillation amplitude was smaller than that simply expected from $2e$ per pulse, $2e/T_r = 20$ pA. The finite rise and fall times of the pulse might explain this deviation. We recall that in the limit of long rise and fall times (the adiabatic limit), there would be no transition probability to $|2\rangle$. For the realistic rise and fall times of the pulse we assumed in the simulation above, for example, the amplitude of the oscillations in $\langle \Delta P(2) \rangle$ at $Q_0/e = 0.51$ is reduced to ~ 0.4, by which the current signal would be decreased. Moreover, the finite repetition time (not much longer than $\Gamma_{qp1}^{-1} + \Gamma_{qp2}^{-1}$) could also reduce the signal due to the incomplete relaxation of $|2\rangle$ to $|0\rangle$ after each pulse.

To further confirm that the observed oscillation was coherent oscillation due to Josephson coupling, we estimated the Josephson energy E_J from the oscillation period T_{coh} as $E_J = h/T_{coh}$ and investigated its magnetic-field dependence (filled circles in Fig. 4 inset). We also measured E_J in the frequency domain through microwave spectroscopy of the energy-level splitting[4] (open squares in Fig. 4 inset). The two sets of data agreed very well, and fitted the expected cosine curve.

For future application as quantum computing devices[5–7], a crucial parameter is the decoherence time. The main decoherence source in a single-Cooper-pair box is thought to be spontaneous photon emission to the electromagnetic environment[1,5–7], and the decoherence time could exceed 1 μs. But when a probe junction is used, as in our set-up, the 'detection' with quasiparticle tunnelling through the probe junction would be the main source of decoherence. So far, we have observed oscillation up to $\Delta t \approx 2$ ns, although low-frequency background-charge fluctuation degraded the direct current signal and made it difficult to determine the envelope of the decay. A more detailed study of the decoherence time would provide important information for designing solid-state quantum circuits using superconducting single-Cooper-pair boxes. □

1. Bouchiat, V., Vion, D., Joyez, P., Esteve, D. & Devoret, M. H. Quantum coherence with a single Cooper pair. *Physica Scripta T* **76**, 165–170 (1998).
2. Joyez, P., Lafarge, P., Filipe, A., Esteve, D. & Devoret, M. H. Observation of parity-induced suppression of Josephson tunneling in the superconducting single electron transistor. *Phys. Rev. Lett.* **72**, 2458–2461 (1994).
3. Flees, D., Han, S. & Lukens, J. Interband transitions and band gap measurements in Bloch transistors. *Phys. Rev. Lett.* **78**, 4817–4820 (1997).
4. Nakamura, Y., Chen, C. D. & Tsai, J. S. Spectroscopy of energy-level splitting between two macroscopic quantum states of charge coherently superposed by Josephson coupling. *Phys. Rev. Lett.* **79**, 2328–2331 (1997).
5. Shnirman, A., Schön, G. & Hermon, Z. Quantum manipulation of small Josephson junctions. *Phys. Rev. Lett.* **79**, 2371–2374 (1997).
6. Averin, D. V. Adiabatic quantum computation with Cooper pairs. *Solid State Commun.* **105**, 659–664 (1998).
7. Makhlin, Yu., Schön, G. & Shnirman, A. Josephson-junction qubits with controlled couplings. *Nature* **398**, 305–307 (1999).
8. Shedelbeck, G., Wegscheider, W., Bichler, M. & Abstreiter, G. Coupled quantum dots fabricated by cleaved edge overgrowth: from artificial atoms to molecules. *Science* **278**, 1792–1795 (1997).
9. Oosterkamp, T. H. et al. Microwave spectroscopy of a quantum-dot molecule. *Nature* **395**, 873–876 (1998).
10. Bonadeo, N. H. et al. Coherent optical control of the quantum state of a single quantum dot. *Science* **282**, 1473–1476 (1998).
11. Loss, D. & DiVincenzo, D. P. Quantum computation with quantum dots. *Phys. Rev. A* **57**, 120–126 (1998).
12. Kane, B. E. A silicon-based nuclear spin quantum computer. *Nature* **393**, 133–137 (1998).
13. Leggett, A. J. in *Chance and Matter* (eds Souletie, J., Vannimenus, J. & Stora, R.) 395–506 (Elsevier, Amsterdam, 1984).
14. Tesche, C. D. Can a noninvasive measurement of magnetic flux be performed with superconducting circuits? *Phys. Rev. Lett.* **64**, 2358–2361 (1990).
15. Neumann, F., Ingold, G.-L. & Grabert, H. Influence of the environment on charge quantization in small superconducting islands. *Phys. Rev. B* **50**, 12811–12819 (1994).
16. Fulton, T. A., Gammel, P. L., Bishop, D. J., Dunkleberger, L. N. & Dolan, G. J. Observation of combined Josephson and charging effects in small tunnel junction circuits. *Phys. Rev. Lett.* **63**, 1307–1310 (1989).
17. Averin, D. V. & Aleshkin, V. Ya. Resonant tunneling of Cooper pairs in a system of two small Josephson junctions. *JETP Lett.* **50**, 367–369 (1989).

The existence of supercooled liquid water at 150 K

R. Scott Smith & Bruce D. Kay

Environmental Molecular Sciences Laboratory, Pacific Northwest National Laboratory, PO Box 999, Mail Stop K8-88, Richland, Washington 99352, USA

Supercooled water may offer clues to the anomalous properties of its normal liquid state[1]. The supercooled state also shows anomalous thermodynamic and transport properties at low temperatures[2–4]. Although there are several theoretical explanations for this behaviour, no consensus has emerged[1,2,5–12]. Some theories preclude the existence of the supercooled liquid below an apparent thermodynamic singularity at 228 K (refs 2, 7, 9); others are consistent with a continuous region of metastability from the melting point at 273 K to the glass transition temperature at 136 K (refs 6, 8, 13). But the data needed to distinguish between these possibilities have not yet been forthcoming. Here we determine the diffusivity of amorphous ice by studying isotope intermixing in films less than 500 nanometres thick. The magnitude and temperature dependence of the diffusivity is consistent with the idea that the amorphous solid water melts into a deeply metastable extension of normal liquid water before crystallizing at 160 K. This argues against the idea of a singularity in the supercooled regime at ambient pressure.

Water vapour deposited on low-temperature substrates (<140 K) is known to form an amorphous phase, termed amorphous solid water (ASW), that is metastable with respect to crystalline ice[3,4,14]. There is still a debate about whether this amorphous form of water transforms to a metastable liquid above the glass transition temperature at 136 K and before crystallization near 160 K (refs 15–17). Furthermore, if the amorphous solid does melt into a liquid, a question remains as to whether this liquid is a metastable extension of supercooled liquid water or a distinct thermodynamic phase[15–17]. We have recently measured the difference in the vapour pressure

788 NATURE | VOL 398 | 29 APRIL 1999 | www.nature.com